

We are IntechOpen, the world's leading publisher of Open Access books Built by scientists, for scientists

6,900

Open access books available

186,000

International authors and editors

200M

Downloads

Our authors are among the

154

Countries delivered to

TOP 1%

most cited scientists

12.2%

Contributors from top 500 universities



WEB OF SCIENCE™

Selection of our books indexed in the Book Citation Index
in Web of Science™ Core Collection (BKCI)

Interested in publishing with us?
Contact book.department@intechopen.com

Numbers displayed above are based on latest data collected.
For more information visit www.intechopen.com



Technology of 3D Simulation of High-Speed Damping Processes in the Hydraulic Brake Device

Valentin Efremov, Andrey Kozelkov, Sergey Dmitriev, Andrey Kurkin, Vadim Kurulin and Dmitry Utkin

Abstract

This chapter describes a three-dimensional simulation technology for physical processes in concentric hydraulic brakes with a throttling-groove partly filled hydraulic cylinder. The technology is based on the numerical solution of a system of Navier–Stokes equations. Free surface tracking is provided by the volume of fluid (VOF) method. Recoiling parts are simulated by means of moving transformable grids. Numerical solution of the equations is based on the finite-volume discretization on an unstructured grid. Our technology enables simulations of the whole working cycle of the hydraulic brake. Results of hydraulic brake simulations in the counter-recoil regime are reported. The results of the simulations are compared with experimental data obtained on JSC “KBP” test benches. The calculated and the experimental sets of data are compared based on the piston velocity as a function of distance. The performance of the hydraulic brake is studied as a function of the fluid mass and firing elevation of the gun.

Keywords: hydraulic brake, Navier-stokes equations, multi-phase flow, volume of fluid, moving rigid body, turbulent flow

1. Introduction

This chapter describes our three-dimensional simulation technology for physical processes in hydraulic brakes with a throttling-groove partly filled hydraulic cylinder. The technology is based on the numerical solution of a system of Navier–Stokes equations with an additional transport equation to track the working fluid/free volume interface by the volume of fluid (VOF) method [1, 2]. As a solver, we use an iterative algorithm, PISO [1, 3], combined with a SLAE solver based on the algebraic multigrid method [4]. To improve the accuracy of solution, we use interface capturing schemes, HRIC [1, 4], near the interface between the phases. Moving parts are simulated by means of moving deforming meshes [5], the motion of which is represented in the initial equations with the Lagrange-Eulerian approximation [6]. Our technology enables modeling of the whole working cycle of the hydraulic brake.

To demonstrate the performance of our technology, we are considering simulation of a hydraulic brake with a throttling-groove partly filled hydraulic cylinder. The simulation outputs are compared with experimental data obtained on the

test benches at JSC “KBP.” The calculated and the experimental sets of data are compared based on the piston velocity as a function of displacement. The performance of the hydraulic brake is studied as a function of the fluid mass and hydraulic brake angle.

2. Problem definition

The hydraulic brake serves to absorb the energy of moving parts. Its structure consists of a case with a grooved inner surface, a ring piston mounted directly on the outer surface of the barrel and having holes matching the guide rods with stranded counter-recoil springs uniformly distributed around the barrel in the hydraulic brake chamber, and front and rear packings with circular-cross-section rubber O-rings to seal the hydraulic brake chamber filled with hydraulic fluid (Figure 1).

The hydraulic brake starts to react as soon as there is no more free space in the recoil chamber (space between the piston and the rear packing); the fluid is sprinkled through the gaps from the recoil chamber to the counter-recoil chamber (space between the piston and the front packing) at a growing rate and stops the moving parts.

Recoil of the moving parts is countered by the energy stored by the counter-recoil springs while braking. In the counter-recoil phase, the fluid from the counter-recoil chamber is sprinkled through the gaps into the recoil chamber providing the

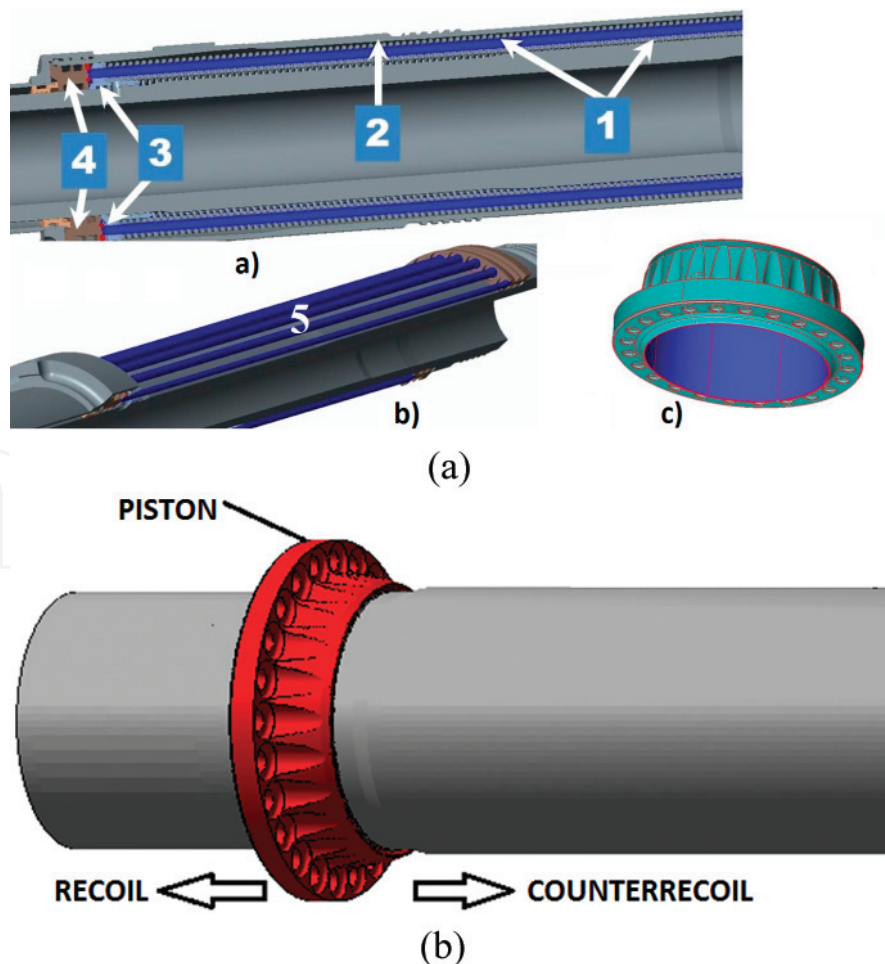


Figure 1.
 (a) General layout of the hydraulic brake: (a) general layout (1—hydraulic fluid cylinder with guides and springs, 2—case, 3—piston, 4—packings); (b) general layout without case (5—guides); and (c) piston;
 (b) schematic of operation.

required counter-recoil braking law. Both for recoil and for counter recoil, the areas of fluid flow in the hydraulic brake are generated by the gaps between the piston and the grooved case surface defining the law of motion, and between the piston holes and the guide rods.

Numerical simulation of the hydraulic brake includes the following physical processes: turbulent flow of fluid encountering sudden contractions, expansions, and axisymmetric gaps; multi-phase flow with different equations of state (it is reasonable to use constant-density approximation for fluid and perfect gas law for air); and flow with moving solids.

The scope of this work included the development of a mathematical model and numerical method to simulate these physical processes.

3. Mathematical model and numerical scheme

Simulation of hydraulic brake operation involves multi-phase flow simulation with two phases. Each phase can have its individual equation of state. Let us assume that the flow is isothermal within one operation cycle and that the phases have the same field of velocity. These assumptions allow us to construct our numerical model using the VOF method [1, 7]. Considering the assumptions above, let us describe the flow of matter by a system of equations, comprised of the mass and momentum equations and the volume fraction transfer equation:

$$\begin{cases} \frac{\partial \rho}{\partial t} + \frac{\partial}{\partial x_i} (\rho u_i) = 0, \\ \frac{\partial \rho u_i}{\partial t} + \frac{\partial}{\partial x_i} (\rho u_i u_j) = -\frac{\partial p}{\partial x_i} + \frac{\partial}{\partial x_i} \tau_{ij} + \rho g_i, \\ \frac{\partial \rho_\xi \alpha_\xi}{\partial t} + \frac{\partial}{\partial x_i} (u_i \rho_\xi \alpha_\xi) = 0, \end{cases} \quad (1)$$

where t is the time, $u_i = \{u_1, u_2, u_3\} = \{u, v, w\}$ is the velocity, x_i is the spatial vector component, τ_{ij} is the viscous stress tensor, g_i is the gravity acceleration vector, ξ is the phase index, α_ξ is the volume fraction of the ξ -th phase, and ρ is the resulting density defined as an average over all the phases:

$$\rho = \sum_{\xi=1}^N \rho_\xi \alpha_\xi \quad (2)$$

where N is the number of phases.

The volume fraction transfer equation is written in terms of the transfer of the quantity α_ξ :

$$\frac{\partial \alpha_\xi}{\partial t} + \frac{\partial}{\partial x_i} (u_i \alpha_\xi) = -\frac{\alpha_\xi}{\rho_\xi} \left(\frac{\partial \rho_\xi}{\partial t} + u_i \frac{\partial \rho_\xi}{\partial x_i} \right) \quad (3)$$

Summing Eq. (3) over all the phases and considering the equality $\sum_\xi \alpha_\xi = 1$, we obtain the following mass equation with respect to the velocity divergence:

$$\frac{\partial u_i}{\partial x_i} = -\sum_\xi \frac{\alpha_\xi}{\rho_\xi} \left(\frac{\partial \rho_\xi}{\partial t} + u_i \frac{\partial \rho_\xi}{\partial x_i} \right) = -\sum_\xi \frac{\alpha_\xi}{\rho_\xi} \frac{d\rho_\xi}{dt} \quad (4)$$

The momentum equation is written in a half-divergent form. This stabilizes the iterative procedure of numerical solution of this equation [3, 4]:

$$\rho \frac{\partial u_i}{\partial t} + \frac{\partial}{\partial x_j} (\rho u_i u_j) - u_i \frac{\partial}{\partial x_j} (\rho u_j) = -\frac{\partial p}{\partial x_i} + \frac{\partial \tau_{ij}}{\partial x_j} + \rho g_i \quad (5)$$

An important feature of this problem is that we need to consider the motion of moving parts, which travel to a distance exceeding the half length of the hydraulic brake during computation. To incorporate their motion, we decided to use a topology-preserving mesh deformation method. To prevent unnecessary cell deformations, the mesh nodes located at fixed elements (case and guide rods) follow the moving piston preserving their geometry. The mesh deformation was implemented by the IDW method [5].

To allow for the mesh motion in Eq. (1), we have rewritten the equations of volume fraction transfer and momentum of the phases in a moving frame of coordinate in accordance with the known law [6]:

$$\frac{d^* \varphi}{dt} = \frac{\partial \varphi}{\partial t} + v_i \frac{\partial \varphi}{\partial x_i} \quad (6)$$

where $\frac{d^* \varphi}{dt}$ is the substantial derivative φ with respect to the moving frame of reference and v_i is the mesh displacement velocity vector. Using Eq. (3), the volume fraction transfer equation can be written as:

$$\frac{d^* \alpha_\xi}{dt} + (u_i - v_i) \frac{\partial \alpha_\xi}{\partial x_i} + \alpha_\xi \frac{\partial u_i}{\partial x_i} = -\frac{\alpha_\xi}{\rho_\xi} \left[\frac{d^* \rho_\xi}{dt} + (u_i - v_i) \frac{\partial \rho_\xi}{\partial x_i} \right] \quad (7)$$

Here $\frac{d^* \alpha_\xi}{dt}$ denotes the substantial derivative on the moving mesh. The momentum equation is also defined with respect to the moving frame of reference considering Eq. (3):

$$\rho \frac{d^* u_i}{dt} + \frac{\partial}{\partial x_j} (\rho u_i (u_j - v_j)) - u_i \frac{\partial}{\partial x_j} (\rho (u_j - v_j)) = -\frac{\partial p}{\partial x_i} + \frac{\partial \tau_{ij}}{\partial x_j} + \rho g_i \quad (8)$$

The mass equation is defined with respect to the velocity in the moving frame of reference:

$$\frac{\partial (u_i - v_i)}{\partial x_i} = -\sum_\xi \frac{\alpha_\xi}{\rho_\xi} \left[\frac{d^* \rho_\xi}{dt} + (u_i - v_i) \frac{\partial \rho_\xi}{\partial x_i} \right] \quad (9)$$

This form of the equations is easy to implement within the framework of finite-volume discretization [8–11]. The chosen way of taking into account the mesh motion is optimal, because it does not require topology reconstruction, though conservative with respect to the major quantities.

The experimental data on the hydraulic brake operation make it possible to estimate the Reynolds number, which equals $Re = 10^5 - 10^6$ in the cylindrical gap during recoil of the moving parts. The most reasonable way to include turbulent flow components with such a Reynolds number is to use the RANS approach based on the solution of the Reynolds-averaged system Eq. (2) [8, 9]. The averaged system of equations is closed using the SST turbulence model, which has proven its efficiency in real-life problem simulations [11–13]. In the SST model, the $(k-\varepsilon)$ model is formulated in terms of $(k-\omega)$ and is focused on resolving small-scale turbulence in the outer flow region. A $(k-\omega)$ model intended to describe large-scale turbulence is used in the boundary layer. The combination of these models together is carried out with the help of a function that ensures the proximity of the total model to the $(k-\varepsilon)$ model far from the solid walls and to the $(k-\omega)$ model in the near-wall flow area.

The resulting system of equations is solved by numerical integration on the finite-volume mesh. The relationship of pressure and velocity while solving Eq. (1) is determined by the SIMPLE algorithm [2]. The SIMPLE algorithm allows to find the pressure field for closure of the continuity equation. Let us write the equation of conservation of momentum at time discretization according to the Euler scheme:

$$\rho \frac{u_i^{n+1} - u_i^j}{\Delta t} + \rho \frac{\partial}{\partial x_j} (u_i^{n+1} u_j^n) = - \frac{\partial p^{n+1}}{\partial x_i} + \frac{\partial}{\partial x_j} (\tau_{ij}^{n+1}) \quad (10)$$

where n is the solution from the previous iteration, and j is the solution from the previous time step. To solve this equation, the pressure and velocity are supposed to have the form:

$$\begin{cases} u_i^{n+1} = u_i^n + u_i^*, \\ p^{n+1} = p^n + \alpha_p (p^{n+1} - p^n) = p^n + \alpha_p \delta p^{n+1}. \end{cases} \quad (11)$$

Here $0 \leq \alpha_p \leq 1$ is the parameter of relaxation.

Substitution of the first expression in Eq. (11) into Eq. (10) yields a preliminary estimate of the velocity value in the next step from the equation:

$$\rho \frac{u_i^*}{\Delta t} + \rho \frac{\partial}{\partial x_j} (u_i^* u_j^n) - \frac{\partial}{\partial x_j} (\tau_{ij}^*) = \rho \frac{u_i^j}{\Delta t} - \frac{\partial p^n}{\partial x_i} \quad (12)$$

The molecular and turbulent components of the tensor of tangential stress in Eq. (12) are also calculated using u_i^* . In the second stage, the full speed value at the $(n + 1)$ th iteration is calculated by adjustment using the correction to pressure:

$$u_i^{n+1} = u_i^* - \Delta t \frac{\partial(\delta p^{n+1})}{\partial x_i} \quad (13)$$

The pressure correction is found from Eq. (13) using the continuity condition for u_i^{n+1} . Taking the derivative of both sides of Eq. (13), we obtain the Poisson equation for pressure:

$$\frac{\partial}{\partial x_i} \left(\frac{\partial(\delta p^{n+1})}{\partial x_i} \right) = \frac{1}{\Delta t} \frac{\partial u_i^*}{\partial x_i} \quad (14)$$

This iterative procedure allows to obtain fields of velocity and pressure satisfying the system of Eq. (1).

Discretization of the equations is performed by a finite-volume technology. Let us show it on the example of the equation of transfer of a scalar quantity φ :

$$\frac{\partial \rho \varphi}{\partial t} + \frac{\partial}{\partial x_j} (\rho \varphi u_j) = \frac{\partial}{\partial x_j} \tau_j + Q, \quad \tau_j = \mu \frac{\partial \varphi}{\partial x_j} \quad (15)$$

The time discretization of Eq. (15) can be carried out using one of the known schemes, for example, the Euler scheme, which is used in the work to solve non-stationary problems using the RANS approach:

$$\frac{\rho^{j+1} \varphi^{j+1} - \rho^j \varphi^j}{\Delta t} + \left[\frac{\partial}{\partial x_j} (\rho \varphi u_j) - \frac{\partial}{\partial x_j} \tau_j - Q \right]^{j+1} = 0 \quad (16)$$

Here j is the number of the time step.

Let us integrate Eq. (16) over volume and proceed to integration over the area for the convective and diffusion terms:

$$\int_{V_p} \frac{\rho^{j+1}\varphi^{j+1} - \rho^j\varphi^j}{\Delta t} dV + \oint_{S_p} \rho\varphi u_j dS_j - \oint_{S_p} \mu \frac{\partial\varphi}{\partial x_j} dS_j - \int_{V_p} Q dV = 0 \quad (17)$$

For approximation on a finite-volume grid, the convective term can be written in the form:

$$\oint_{S_p} \rho\varphi u_j dS_j \approx \sum_k \rho_k \varphi_k u_{j,k} S_{j,k} \approx \sum_k \rho_k \varphi_k F_k \quad (18)$$

where F_k is the volume flow through the face k . The value of φ_k on the face k is determined by the applied convective scheme.

The discrete analog of the diffusion term can be written in the following form:

$$\oint_{S_p} \mu \frac{\partial\varphi}{\partial x_j} dS_j \approx \sum_k \left(\mu \frac{\partial\varphi}{\partial x_j} \right)_k S_{j,k} = \sum_k \mu_k \left(\frac{\partial\varphi}{\partial n_k} \right)_k |S_k| \quad (19)$$

where n_k is the normal to face k .

The value of $\left(\frac{\partial\varphi}{\partial x_i} \right)_k$ on the face k is found by linear interpolation on the values of the gradient in the cells, which are determined by one of the known methods, for example, the Gauss method:

$$\left(\frac{\partial\varphi}{\partial x_i} \right)_P = \frac{1}{V_P} \sum_k \varphi_k S_{k,i} \quad (20)$$

Using this discretization, Eq. (15) is replaced by a system of linear algebraic equations written for each calculation cell:

$$A_P \varphi_P + \sum_{k_{\text{int}}} A_{k_{\text{int}}} \varphi_{M_{k_{\text{int}}}} = R_{i,P} \quad (21)$$

Time discretization of the equations is performed by a three-layer second-order scheme [10]. Discretization of the convective terms in the equation of motion, equation of transfer of turbulent parameters, is performed by the upwind scheme LUD [10], and in the volume fraction transfer equation, by the HRIC scheme [1], which prevents excessive numerical diffusion of the phase interface. The force of gravity was included using a bulk force fitting algorithm [14].

These methods and models have been implemented in the software package LOGOS. LOGOS is a 3D multi-physics code for convective heat and mass transfer, aerodynamic and hydrodynamic simulations on parallel computers [11, 13–18]. LOGOS has been successfully verified and demonstrated with sufficiently high efficiency on a number of various hydrodynamic tests, including propagation of gravity waves on a free surface (tsunami) [2, 14, 18] and industry-specific simulations [11, 15]. Speedup of computations on highly parallel computers is provided by an original implementation of the algebraic multigrid method [11, 19].

4. Numerical simulation of hydraulic brake operation

Let us consider the counter-recoil phase in the operation of the hydraulic brake, when the moving parts together with the piston (see **Figure 1b**) are driven by the

springs from their rightmost position to the leftmost one resisting the hydrodynamic force acting on the fluid side.

To solve the problem numerically, an unstructured hexahedral-dominant mesh was constructed using the pre- and post-processing tools of the LOGOS. The mesh is refined near the piston and in the gaps between the piston and the case, where the flow of fluid is particularly strong. **Figure 2** shows mesh fragments.

When constructing the mesh, we placed the piston in the middle between its rightmost initial and leftmost end positions of counter recoil. This minimizes mesh deformation during computation. The problem was simulated in the unsteady setup; the time step was $5 \times 10^{-4} t_0$, where t_0 is the total time of piston counter-recoil motion. The forces acting on the piston, its velocity and displacement were calculated at the end of each time step after finding the solution of the Navier–Stokes equation.

During computation, the piston together with the moving parts is accelerated by the springs and reaches its maximum velocity during the second half of its travel. The piston then enters the grooved region of the case with a decreasing gap, as a result of which the hydrodynamic resistance grows and slows down the moving parts. The computation ends when the piston is at $d_m = 0.01$ m from its end position, which is attributed to the maximum admissible mesh deformation in the counter-recoil chamber.

When the piston is moving, in addition to the force exerted by the springs and hydrodynamic resistance, the moving parts are exposed to friction arising in the packings, between the guides and the piston, and inside the stranded springs during their compression or tension. The resultant of the forces exerted by the springs and friction can be expanded into two components. The first does not depend on the velocity of the moving parts and can be easily measured experimentally by pulling the moving parts at a slow rate. The second depends on the velocity of the moving parts and is mostly related to friction in the turns of the stranded springs. Empirical estimates show that the second component of the resultant force can be expressed empirically as

$$F_{mp}^{din} = \eta u M \quad (22)$$

where u is the velocity, M is the mass of the moving parts, η is an empirical coefficient, which can vary in the range of $\eta = 0-5 \text{ s}^{-1}$ for the springs we use.

Computations were conducted with $\eta = 0, 3, 4,$ and 5 . **Figure 3** shows the field of volume fraction of the fluid at different times for $\eta = 0 \text{ s}^{-1}$.

At $t = 0.2 t_0$, where t_0 is the total time of counter recoil, a wave of fluid rises upstream of the piston. Pressure in the counter-recoil chamber grows. Air is actively bled over through the upper part of the gap. A flow of fluid emerges in the bottom part of the gap. Its rate is 10–15 times slower than the rate of the air flow (**Figure 4**).

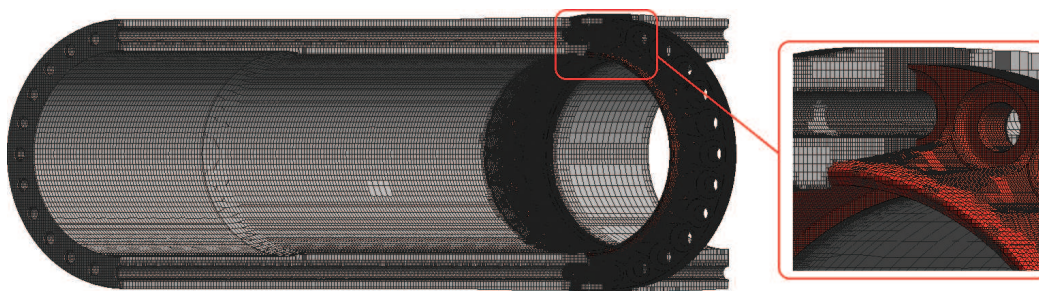


Figure 2.
Mesh fragments.

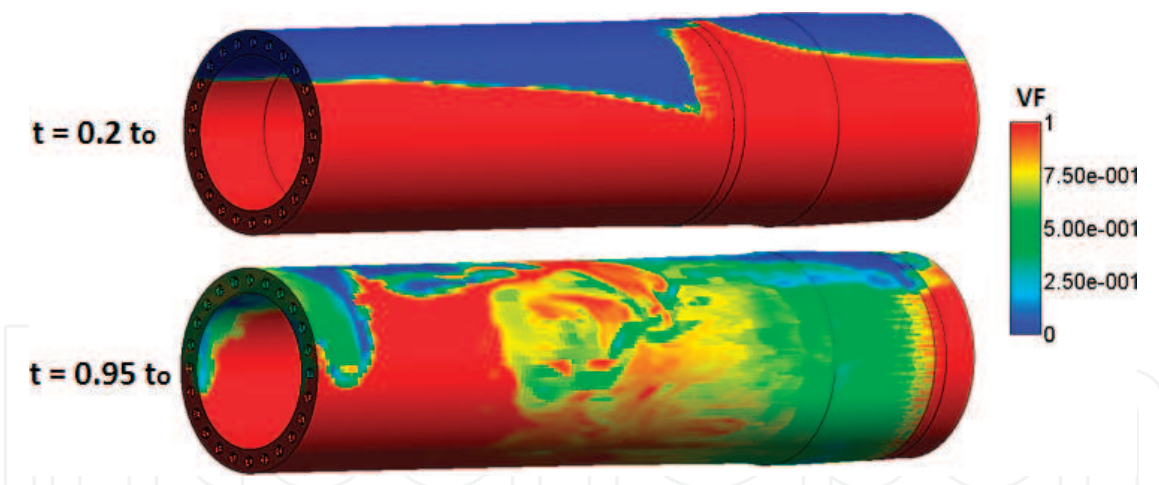


Figure 3.
Field of volume fraction of the fluid at different times.

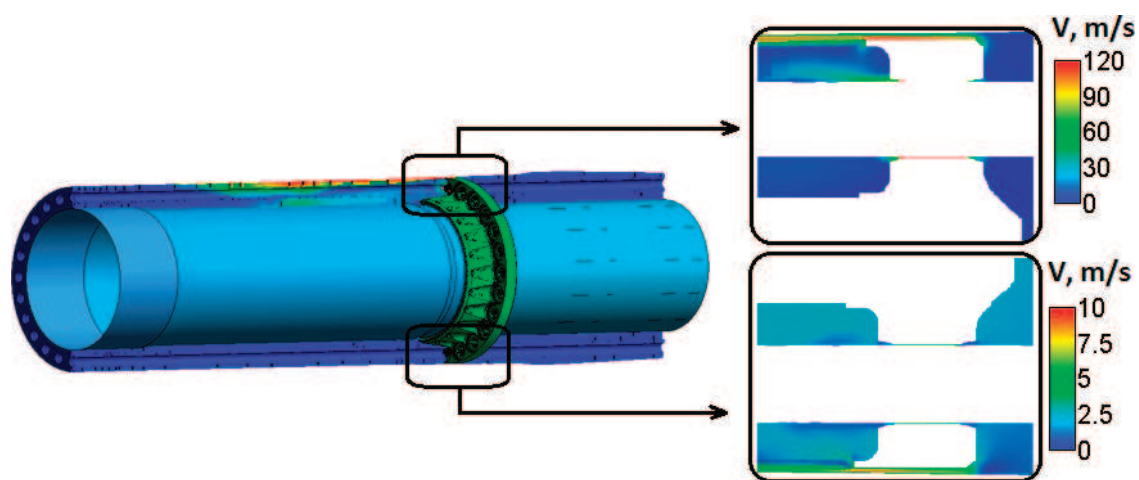


Figure 4.
Field of velocity amplitude ($t = 0.2 t_0$).

As the piston continues to move, the fluid is sprinkled through the gaps at a growing rate. At $t = 0.95 t_0$, most of the fluid is already pressed out of the counter-recoil chamber; it forms a nearly homogeneous gas–liquid mixture in the opposite chamber. Pressure in the counter-recoil chamber reaches $P = 150 P_0$, where $P_0 = 1 \text{ atm}$ is the initial pressure.

Fluid velocity in the gap grows as high as $V = 50\text{--}70 \text{ m/s}$ (**Figure 5**). After the fluid has flown over through the gap, the bulk gas content in the mixture increases steeply as a result of a pressure drop. This leads to a further growth of mixture velocity to $V = 90 \text{ m/s}$ (**Figure 5**). This effect is less pronounced in the bottom part of the gap because of the lower gas content in the mixture sprinkled through the gap.

Figure 6 shows a plot of piston velocity as a function of displacement for different values of η .

On the whole, our results match the experimental data both qualitatively and quantitatively. All the simulated cases consistently predict the state of piston acceleration. In the high-velocity phase of piston motion, the parameter η starts to play a significant role. The best agreement with experiment is provided by $\eta = 3 \text{ s}^{-1}$. This does not mean that the value above is close to the actual one, but is indicative of the fact that our numerical model, input data, and mesh are capable of describing the process of piston motion with required accuracy, if we use this value of η in our computational model.

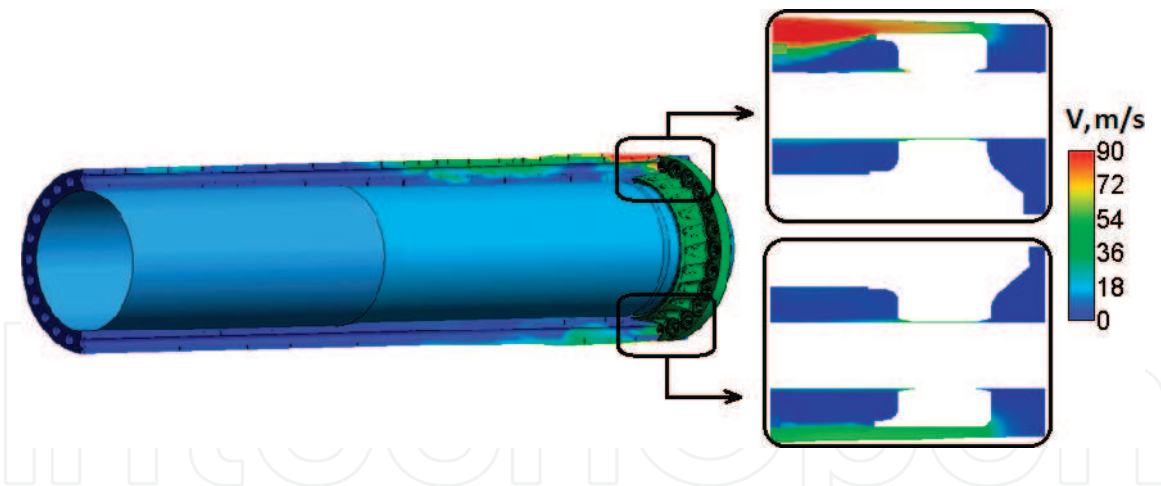


Figure 5.
 Field of velocity amplitude ($t = 0.95 t_0$).

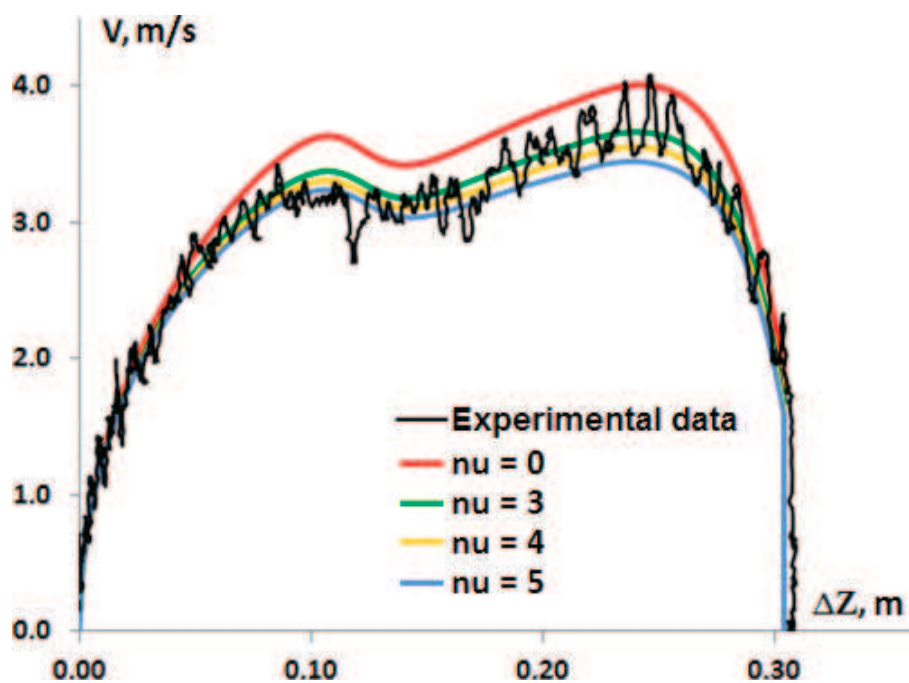


Figure 6.
 Piston velocity as a function of displacement.

The counter-recoil phase occurs at zero angle (the hydraulic brake is placed horizontally). Let us consider the dependence of piston motion on the accuracy of horizontal positioning of the hydraulic brake. For this purpose, let us carry out calculations with angles $\alpha = 1^\circ$ and $\alpha = -1^\circ$. The calculation results are shown in **Figure 7**.

The plots demonstrate that the piston velocity grows with increasing angle. This is quite predictable, because the amount of fluid in the counter-recoil chamber decreases as the angle increases. One should also note that the gravity force acting on the moving parts in the direction opposite to that of their motion at $\alpha > 0$ or in the direction of their motion at $\alpha < 0$ has no measurable effect on the result.

The angle of the hydraulic brake also controls the static pressure in the counter-recoil chamber (**Figure 8**). The first pressure maximum is attributed to a decrease in the volume fraction of air in the counter-recoil chamber as the piston moves, and the subsequent drop, to a growth in the gap size between the piston and the grooved case region. As the angle increases, the initial amount of fluid in the counter-recoil chamber decreases, and the maximum shifts toward the range of greater piston

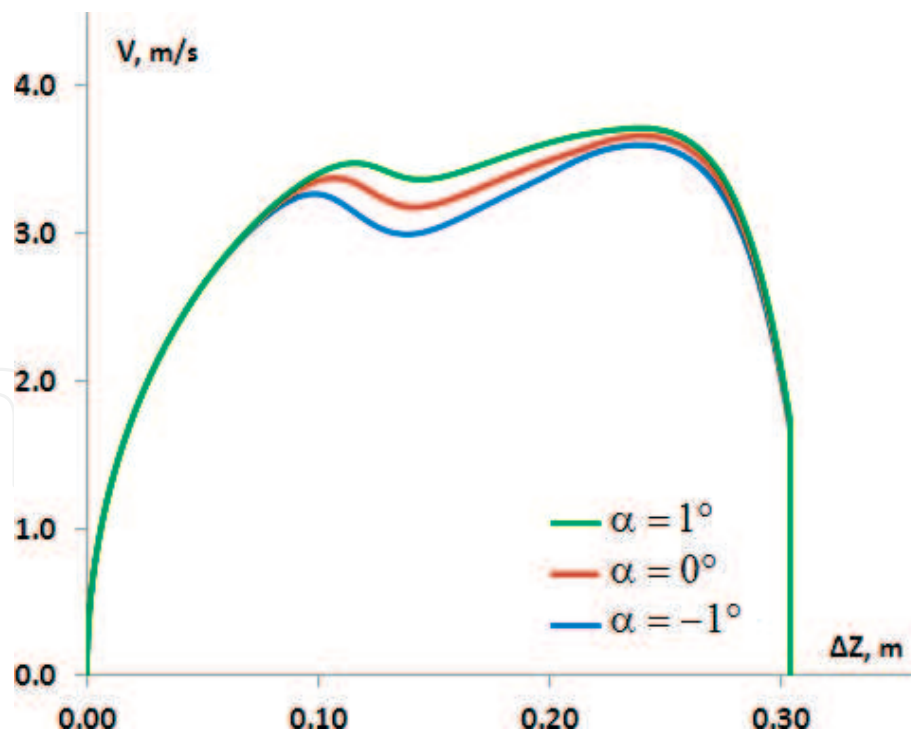


Figure 7.
Piston velocity as a function of piston displacement for different angles.

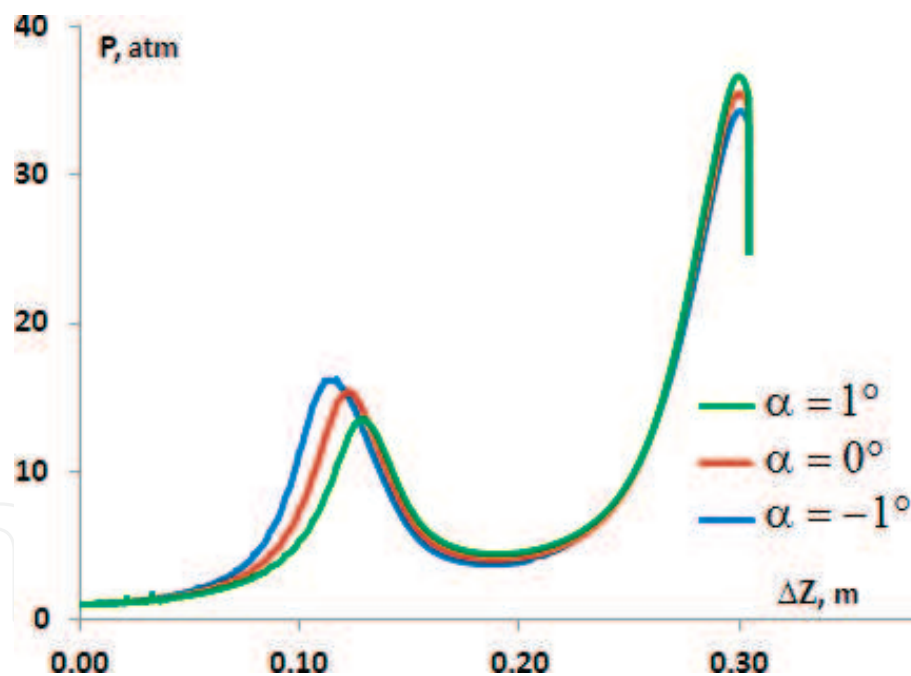


Figure 8.
Static pressure in the counter-recoil chamber as a function of piston displacement.

displacements, which allows the piston to speed up to a higher velocity. This increase in the piston velocity leads to a higher pressure maximum in the region of strong slowdown (the second pressure maximum in **Figure 6**). Thus, an increase in the amount of fluid in the counter-recoil chamber leads to a higher and earlier first pressure maximum and a lower second pressure maximum, which is quite consistent with process physics.

The results of piston motion analysis as a function of initial fluid level in the hydraulic brake ($h = h_0$, $h = h_0 + 0.01$ m, $h = h_0 - 0.01$ m) are shown in **Figure 9**.

The fluid level has a considerable effect on the piston velocity. A 1-cm increase in the level results in a 10% drop in the average piston velocity, which is explained

by a decrease in the force of hydrodynamic resistance acting on the moving parts. Note that the slopes of the velocity plot are indicative of the same trend: as the fluid level in the counter-recoil chamber rises, the first pressure maximum increases and the second one decreases.

An important characteristic of the counter-recoil piston motion is piston velocity V_{extr} at 159 mm to the counter-recoil end ($\Delta Z = 153$ mm), where the shell extractor is located, the performance of which depends on the velocity of the moving parts. Another important characteristic is piston velocity close to the end position V_{end} , which will govern the force exerted by the piston on the packing in the counter-recoil chamber. The values of these characteristics are presented in **Table 1**.

The table demonstrates that a change in the fluid level within 1 cm leads to a 15% change in the velocity V_{extr} . A change in the angle to 1 degree results in a 5% change in the velocity. Note that the level and angle variations have a minor effect on the velocity V_{end} , the oscillations of which do not exceed 2–3%.

The results demonstrate that the governing quantity, which controls the performance of the hydraulic brake, is the initial fluid level in the counter-recoil chamber. An increase in the fluid level results in a lower average piston velocity, smaller V_{extr} and V_{end} , shift and rise in the first pressure maximum, and drop in the second pressure maximum. The process pattern, however, does not depend on the reason

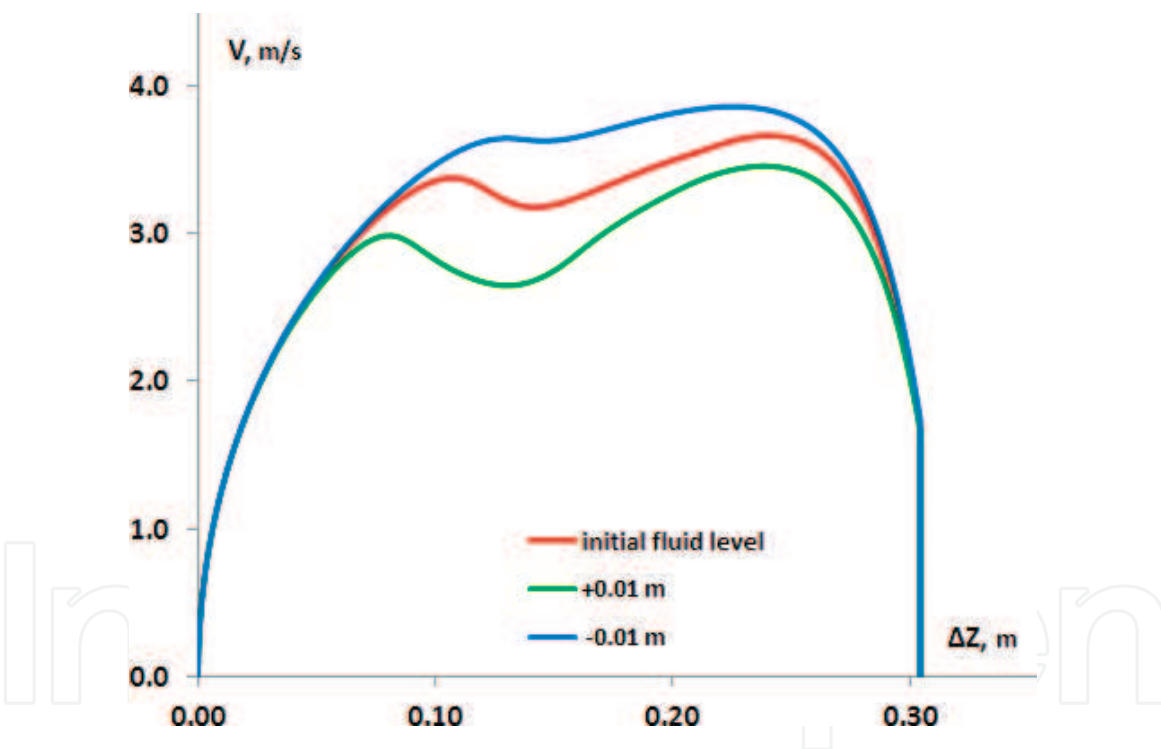


Figure 9.
 Piston velocity as a function of displacement for different fluid levels.

No.	α [degree]	$h - h_0$ [sm]	V_{extr} [m/s]	V_{end} [m/s]
1	0.0	-1.0	3.64	1.74
2	0.0	0.0	3.21	1.69
3	0.0	1.0	2.78	1.65
4	-1.0	0.0	3.05	1.66
5	1.0	0.0	3.38	1.72

Table 1.
 Piston motion characteristics.

of the rise in the fluid level in the counter-recoil chamber: both general increase in the initial amount of fluid and negative angle of the hydraulic brake result in the same trends.

5. Conclusion

In this chapter, we have presented a three-dimensional numerical modeling technology for physical processes occurring in hydraulic brake devices. The technology is based on the numerical solution of a system of Reynolds-averaged Navier-Stokes equations. To track the free surface, we use the volume of fluid (VOF) method. Moving parts are simulated by means of moving deforming meshes. Numerical solution of the equations is based on the finite-volume discretization, which is used to model the counter-recoil phase in hydraulic brake operation. This technology enables simulations on three-dimensional unstructured meshes. The technology is implemented based on the program package LOGOS, which provides high parallel efficiency of simulations.

The technology has been used to model the counter-recoil phase in hydraulic brake operation. Results of studying the effect of the parameter related to friction, hydraulic brake angle, and initial fluid level are reported. Our numerical experiments have demonstrated that the initial fluid level in the counter-recoil chamber is the governing quantity in hydraulic brake operation. An increase in the fluid level in the counter-recoil chamber as a result of pouring more fluid or placing the hydraulic brake at a negative angle results in the same trend in the change in pressure and its maximums.

Acknowledgements

This research has been funded by grants of the President of the Russian Federation for state support of research projects by young doctors of science (MD-4874.2018.9) and state support of the leading scientific schools of the Russian Federation (NSh-2685.2018.5), and supported financially by the Russian Foundation for Basic Research (project No. 16-01-00267).

Conflict of interest

The authors declare that they have no conflict of interest.

IntechOpen

Author details

Valentin Efremov¹, Andrey Kozelkov², Sergey Dmitriev³, Andrey Kurkin^{3*},
Vadim Kurulin² and Dmitry Utkin²

¹ Joint-Stock Company “Instrument Design Bureau named after Academician A.G. Shipunov”, Tula, Russia

² Russian Federal Nuclear Center—All-Russian Research Institute of Experimental Physics, Sarov, Russia

³ Nizhny Novgorod State Technical University n.a. R.E. Alekseev, Nizhny Novgorod, Russia

*Address all correspondence to: aakurkin@gmail.com

IntechOpen

© 2018 The Author(s). Licensee IntechOpen. This chapter is distributed under the terms of the Creative Commons Attribution License (<http://creativecommons.org/licenses/by/3.0>), which permits unrestricted use, distribution, and reproduction in any medium, provided the original work is properly cited. 

References

- [1] Ubbink O. Numerical prediction of two fluid systems with sharp interfaces [thesis]. London: Imperial College of Science, University of London; 1997
- [2] Kozelkov AS, Kurkin AA, Pelinovsky EN, Tyatyushkina ES, Kurulin VV, Tarasova NV. Landslide-type tsunami modelling based on the Navier-stokes equations. *Science of Tsunami Hazards*. 2016;**35**:106-144
- [3] Yatsevich SV, Kurulin VV, Rubtsova DP. On the Application of the PISO Algorithm to Molecular-Immiscible Fluid Dynamics Problems. *VANT, Ser. Matematicheskoe Modelirovanie Fizicheskikh Protsessov*. Vol. 1. 2015. pp. 16-29
- [4] Khrabry AI, Smirnov EM, Zaytsev DK. Solving the convective transport equation with several high-resolution finite volume schemes. Test computations. In: *Proceedings of the 6th International Conference on Computational Fluid Dynamics (ICCFD-6)*; 12–16 July 2010; Russia. Berlin, Heidelberg: Springer-Verlag; 2011. pp. 535-540
- [5] Luke E, Collins E, Blades E. A fast mesh deformation method using explicit interpolation. *Journal of Computational Physics*. 2012;**231**:586-601. DOI: 10.1016/j.jcp.2011.09.021
- [6] Loitsyansky LG. *Liquid and Gas Mechanics*. Vol. 840. Moscow: Nauka; 1987
- [7] Rusche H. Computational fluid dynamics of dispersed two-phase flows at high phase fractions [thesis]. London: Imperial College of Science, University of London; 2002
- [8] CAJ F. Computational techniques for fluid dynamics. In: *Fundamental and General Techniques*. 2nd ed. Vol. 1. Berlin, Heidelberg, New York: Springer-Verlag; 1991. p. 401
- [9] Fletcher CAJ. Computational techniques for fluid dynamics. In: *Specific Techniques for Different Flow Categories*. Vol. 2. Berlin, Heidelberg, New York: Springer-Verlag; 1998. p. 496
- [10] Jasak H. Error analysis and estimation for the finite volume method with applications to fluid flows [thesis]. London: Imperial College of Science, University of London; 1996
- [11] Kozelkov AS, Kurulin VV, Lashkin SV, Shagaliev RM, Yalozo AV. Investigation of supercomputer capabilities for the scalable numerical simulation of computational fluid dynamics problems in industrial applications. *Computational Mathematics and Mathematical Physics*. 2016;**56**:1506-1516. DOI: 10.1134/S0965542516080091
- [12] Menter FR, Kuntz M, Langtry R. Ten years of experience with the SST turbulent model. In: Hanjalic K, Nagano Y, Tummers M, editors. *Turbulence, Heat and Mass Transfer 4*. Danbury: Begell House Inc; 2003. pp. 625-632
- [13] Kozelkov A, Kurulin V, Emelyanov V, Tyatyushkina E, Volkov K. Comparison of convective flux discretization schemes in detached-eddy simulation of turbulent flows on unstructured meshes. *Journal of Scientific Computing*. 2016;**67**:176-191. DOI: 10.1007/s10915-015-0075-7
- [14] Efremov VR, Kozelkov AS, Kornev AV, Kurkin AA, Kurulin VV, Strelets DY, et al. Method for taking into account gravity in free-surface flow simulation. *Computational Mathematics and Mathematical Physics*. 2017;**57**: 1720-1733. DOI: 10.1134/S0965542517100086

[15] Deryugin YN, Zhuchkov RN, Zelenskiy DK, Kozelkov AS, Sarazov AV, Kudimov NF, et al. Validation results for the LOGOS multifunction software package in solving problems of aerodynamics and gas dynamics for the lift-off and injection of launch vehicles. *Mathematical Models and Computer Simulations*. 2015;7:144-153. DOI: 10.1134/S2070048215020052

[16] Kozelkov AS, Kurkin AA, Legchanov MA, Kurulin VV, Tyatyushkina ES, Tsibereva YA. Investigation of the application of RANS turbulence models to the calculation of nonisothermal low-Prandtl-number flows. *Fluid Dynamics*. 2015;50:501-513. DOI: 10.1134/S0015462815040055

[17] Kozelkov AS, Kurkin AA, Kurulin VV, Lashkin SV, Tarasova NV, Tyatyushkina ES. Numerical modeling of the free rise of an air bubble. *Fluid Dynamics*. 2016;51:709-721. DOI: 10.1134/S0015462816060016

[18] Kozelkov AS, Kurkin AA, Pelinovsky EN, Kurulin VV, Tyatyushkina ES. Numerical modeling of the 2013 meteorite entry in Lake Chebarkul, Russia. *Natural Hazards and Earth System Sciences*. 2017;17:671-683. DOI: 10.5194/nhess-17-671-2017

[19] Volkov KN, Kozelkov AS, Lashkin SV, Tarasova NV, Yalozo AV. A parallel implementation of the algebraic multigrid method for solving problems in dynamics of viscous incompressible fluid. *Computational Mathematics and Mathematical Physics*. 2017;57:2030-2046. DOI: 10.1134/S0965542517120119